INTERNATIONAL JOURNAL FOR NUMERICAL METHODS IN FLUIDS, VOL. 7, 857–867 (1987)

ON THE DEVELOPMENT OF TAYLOR VORTICES IN A VERTICAL ANNULUS WITH A HEATED ROTATING INNER CYLINDER

KENNETH S. BALL AND BAKHTIER FAROUK

Department of Mechanical Engineering and Mechanics, Drexel University, Philadelphia, PA 19104, U.S.A.

SUMMARY

A numerical study has been conducted to determine the heat transfer characteristics and flow patterns which develop around a rotating, heated vertical cylinder enclosed within a stationary concentric cylinder. A tall annulus (aspect ratio of 10) with fixed, adiabatic horizontal end-plates and a radius ratio of 0·5 has been considered. Furthermore, the effect that the introduction of buoyancy forces by heating the inner cylinder has on the development of the Taylor vortex flow is examined. It is observed that the formation of the Taylor vortices is delayed until the rotational parameter $\sigma = Gr/Re^2$ has a value below unity for any given Reynolds number Re which is above the critical value Re_{crit} for the formation of Taylor vortices in an isothermal flow. Also, the Taylor cells first appear at the top of the annulus. As σ is gradually decreased below unity, bifurcations to other states are observed. The final structure of the secondary flow is noticeably distorted in the mixed-convection mode, with the size of the Taylor cells varying greatly along the height of the annulus. This distortion diminishes as σ is further decreased, until the isothermal flow pattern is nearly recovered below $\sigma = 0{\cdot}01$.

KEY WORDS Mixed Convection Taylor Vortices Rotating Annulus Bifurcation

INTRODUCTION

Heat transfer from rotating cylindrical bodies occurs in many practical applications, such as the cooling of turbine rotors or electrical motor shafts. Other applications include the cooling of high-speed gas bearings, rotating condensers for sea-water distillation, and spacecraft power plants.[1] These flows also have many geophysical applications, including oceanic and atmospheric circulation, and hence play important roles in developing weather patterns.[2]

A more recent and direct application of this research is improvement in the techniques of chemical vapour deposition (CVD). CVD is an important process often used in semiconductor device fabrication. During this process, the solid products of a vapour phase chemical reaction are deposited on a substrate as a thin film. In one of the more common reactors, the barrel reactor, the substrate is placed on a rotating turret which is enclosed within a bell jar. One of the major factors governing the deposition process is the flow characteristics of the hot gases over the rotating turret.[3]

In the study of the flow between rotating cylinders, the existence of hydrodynamic instabilities also provides a more fundamental objective: the understanding of how and under what circumstances turbulence may arise from laminar instability. Instabilities in laminar flow are often a prelude to transition to turbulence. Because of the wide range of Reynolds (Taylor) numbers for

0271–2091/87/080857–11$05.50

Received 18 May 1986
Revised 22 December 1986

which the Taylor-vortex flow remains stable, it affords the researcher much insight into the growth of disturbances leading to turbulence.[4]

The Taylor-vortex instability has been the subject of much research. G. I. Taylor showed that a critical speed of rotation exists above which appears a stable, secondary mean flow consisting of regularly spaced toroidal vortices (Taylor vortices).[5] Coles[6] provided a strong experimental study considering a wide range of parameters and flow regimes. Much of the existing analytical work and stability analyses is discussed by Chandrasekhar.[7] Recent studies of the Taylor problem have concentrated on the existence of multiple solutions, which have secondary states characterized by a unique wavelength.[8–16] The wavelength that is selected as the primary state depends upon the initial conditions of the flow.[16] Of these studies, those of Benjamin and Mullin[8,9] have provided many experimental results revealing the nature of the Taylor cell evolution. Numerical studies by Cliffe[10] have verified these results and have helped to provide further insights in their meaning. A recent numerical study by Hughes *et al.*[11] has successfully predicted some of the observed secondary flows in the Taylor experiment.

Comparatively little work has been directed toward the study of the mixed-convection flows in a heated vertical cylindrical annulus with the inner cylinder rotating. This flow remains axisymmetric for a wide range of both the Reynolds and Grashof numbers, and is therefore readily accessible to numerical solution. Snyder and Karlsson[17–19] present experimental observations for the small-gap annulus ($d = 0{\cdot}267$ cm, with $2d/(r_i + r_o) \ll 1$) with a radial thermal gradient imposed upon the flow. They report that a spiral form of the Taylor-vortex flow occurs when the gradient across the gap, $\Delta T/d$, exceeds $\pm 5^\circ$ C/cm. This criterion for an axisymmetric flow was observed for the small-gap case. In the present study, the thermal gradients encountered were of the order of 1° C/cm across the 5 cm gap. It is expected that the present flow will also remain axisymmetric, since the critical Taylor number increases with increasing gap width (i.e. the flow becomes more stable). de Vahl Davis and co-workers[20,21] have also studied this problem, concentrating on the overall flow patterns and heat transfer rates, for short and moderate aspect ratios ($\Gamma = 1$ and $\Gamma = 3$). No information regarding flow bifurcation was given.

In this paper, a tall annulus is considered ($\Gamma = 10$), with particular emphasis on the stability of the flow, the mutual interaction of both the buoyancy and rotational effects (qualified by the rotational parameter $\sigma = Gr/Re^2$), and the subsequent effect on the flow patterns, heat transfer rates and transition criteria.

Multiple solutions are seen to exist for the mixed-convection problem. Since the amplification process of instabilities has a strong influence on the final result, a study of the evolution of Taylor vortices can reveal insights into the dynamical selection process.[15] It is known that the amplification process in natural convection flows has distinct differences from that in pressure-driven flows,[22] and a study of the evolution of Taylor vortices in a mixed-convection flow can help to determine the interaction between the buoyancy and centrifugal forces.

MATHEMATICAL FORMULATION

The geometry considered consists of a smooth, heated isothermal vertical cylinder of radius r_i enclosed by a concentric isothermal cylinder of radius r_o to form an annulus. The annulus is capped by smooth, adiabatic horizontal end-plates. Both the outer cylinder and the end-plates are fixed and stationary, whereas the inner cylinder is allowed to rotate. The geometry is specified by the radius ratio $\eta = r_i/r_o$ and the aspect ratio $\Gamma = H/d$, where d is the gap width $r_o - r_i$.

The fluid considered is air, with $Pr = 0{\cdot}7$. The usual Boussinesq approximation is applied. The Boussinesq approximation remains valid in rotating flows when the centrifugally induced pressure difference effects on the density may be neglected. The criterion used to determine this is that the acceleration ratio A, defined as the ratio of the characteristic centrifugal acceleration to the

acceleration due to gravity, should be small compared to unity:

$$A = (\Omega^2 r_i)/g \ll 1. \tag{1}$$

For all results presented, $A < 0{\cdot}03$.

Governing equations

The Navier–Stokes and energy equations, together with the continuity equation, completely describe the physics of the problem. In cylindrical polar co-ordinates, for an axisymmetric flow, the equations are

$$\rho_0\left(\frac{\partial u}{\partial t} + u\frac{\partial u}{\partial r} + w\frac{\partial u}{\partial z} - \frac{v^2}{r}\right) = -\frac{\partial p}{\partial r} + \mu\left(\frac{\partial^2 u}{\partial r^2} + \frac{1}{r}\frac{\partial u}{\partial r}\frac{u}{r^2} + \frac{\partial^2 u}{\partial z^2}\right), \tag{2a}$$

$$\rho_0\left(\frac{\partial v}{\partial t} + u\frac{\partial v}{\partial r} + w\frac{\partial v}{\partial z} + u\frac{v}{r}\right) = \mu\left(\frac{\partial^2 v}{\partial r^2} + \frac{1}{r}\frac{\partial v}{\partial r} - \frac{v}{r^2} + \frac{\partial^2 v}{\partial z^2}\right), \tag{2b}$$

$$\rho_0\left(\frac{\partial w}{\partial t} + u\frac{\partial w}{\partial r} + w\frac{\partial w}{\partial z}\right) = -\frac{\partial p}{\partial z} + \mu\left(\frac{\partial^2 w}{\partial r^2} + \frac{1}{r}\frac{\partial w}{\partial r} + \frac{\partial^2 w}{\partial z^2}\right) + \rho_0\beta(T - T_0)g, \tag{2c}$$

$$\rho_0 c_p\left\{\frac{\partial T}{\partial t} + u\frac{\partial T}{\partial r} + w\frac{\partial T}{\partial z}\right\} = k\left\{\frac{\partial^2 T}{\partial r^2} + \frac{1}{r}\frac{\partial T}{\partial r} + \frac{\partial^2 T}{\partial z^2}\right\}, \tag{3}$$

$$\frac{\partial u}{\partial r} + \frac{u}{r} + \frac{\partial w}{\partial z} = 0. \tag{4}$$

The equations (2)–(4) are cast into the stream-function–vorticity form by introducing the stream function ψ and vorticity ω as follows:

$$u = -\frac{1}{\rho r}\frac{\partial \psi}{\partial z}, \quad w = \frac{1}{\rho r}\frac{\partial \psi}{\partial r}, \tag{5a),(5b)}$$

$$\omega = \frac{\partial u}{\partial z} - \frac{\partial w}{\partial r}. \tag{6}$$

The equations are made dimensionless by using the gap width d as the length scale, d^2/ν as the time scale (where ν is the kinematic viscosity), and the temperature difference $(T_i - T_0)$.

Boundary conditions

The value of the stream function ψ along all boundaries must be a constant, owing to the no-slip condition at an impermeable wall. This value is taken to be zero. The swirl velocity component is equal to zero at the end-plates and the outer cylinder, which are stationary. The inner cylinder rotates with an angular speed of $\Omega\,(s^{-1})$. The non-dimensional temperature is $T = 1$ at the inner wall and $T = 0$ at the outer wall (which are both isothermal). Both end-plates are taken to be adiabatic. An expression for the vorticity boundary condition can be obtained by expanding the stream function near the surface using a three-term Taylor series expansion and by making use of the continuity and no-slip conditions:

$$\left(\frac{\omega}{r}\right)_{\text{wall}} = \frac{-2{\cdot}0\psi_{nw}}{(\Delta n)^2 (r_w)^2}, \tag{7}$$

where ψ_{nw} is the value of ψ at the near-wall node (adjacent to the wall), Δn is the non-dimensional

distance of the near-wall node from the wall, and r_w is the value of the radial co-ordinate at the wall node being calculated.

Solution procedure

The resulting four coupled elliptic equations (for stream function, vorticity, swirl velocity and temperature) are transformed into difference equations by using a control-volume-based finite difference method. A line-by-line tridiagonal matrix algorithm is employed for the solution of the discretized equations. A $111 \times 21 (z \times r)$ grid is used for the numerical computations with uniform spacing in the z direction and non-uniform spacing in the radial direction. A fully implicit scheme was used to obtain the transient solutions. All computations were performed on a VAX-11/750 computer.

RESULTS AND DISCUSSION

Solutions are obtained for a wide range of the Grashof number ($0 \leqslant Gr \leqslant 10^5$) with the Reynolds number held fixed at $Re = 100$. This value of Re corresponds to a Taylor number $Ta = 9{\cdot}93 \times 10^4$, which is well above the theoretical value $Ta_{crit} = 3{\cdot}310 \times 10^4$ for this geometry.[7] The corresponding range of the rotational parameter $\sigma = Gr/Re^2$ is $0{\cdot}0 \leqslant \sigma \leqslant 10$. This parameter is a densiometric Froude number, and gives the relative importance of the buoyancy and rotational effects. The flow characteristics are found to be primarily dependent on σ. The problem geometry is shown in Figure 1.

Solutions are presented first for the isothermal flow case ($Gr = 0 = \sigma$). Below a critical Reynolds (Taylor) number, the flow is essentially one-dimensional, consisting of concentric circular streamlines in the $(r-\phi)$ plane. The u and w components of velocity (in the r and z directions) are

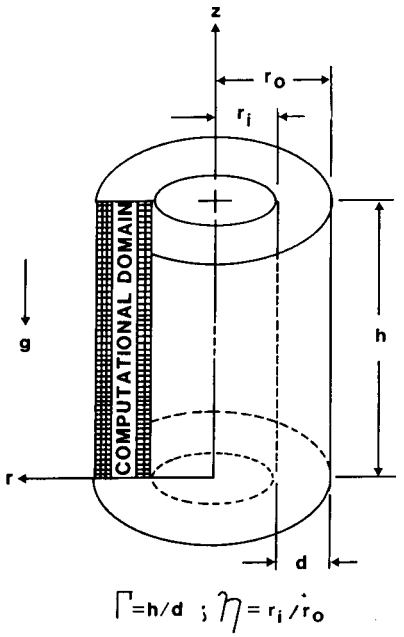

Figure 1. Problem geometry

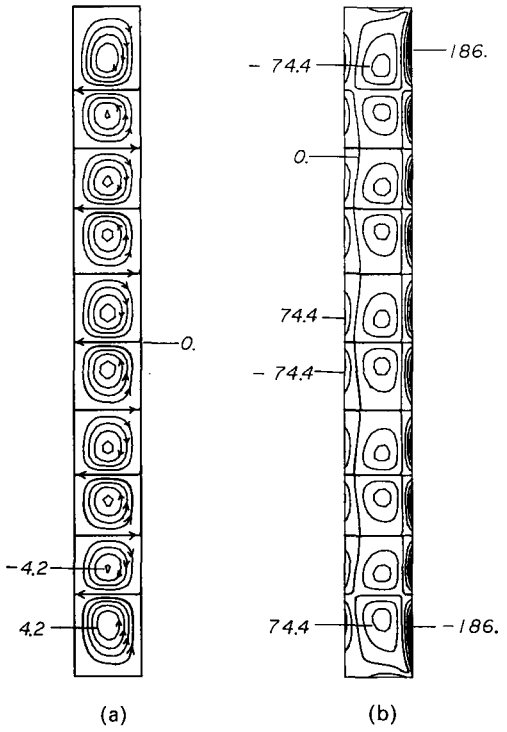

Figure 2. (a) Streamlines, $\pm \Delta\psi = 1{\cdot}1$, and (b) vorticity field, $\pm \Delta\omega = 37{\cdot}2$, for $Re = 100$, $\sigma = 0{\cdot}0$

essentially zero, although a very slight circulation is induced in the $(r-z)$ plane due to the vorticity introduced into the flow by the stationary end-plates. Above a critical Reynolds (Taylor) number, the flow undergoes a transition to a quasi-three-dimensional (axisymmetric) flow characterized by counter-rotating toroidal vortices (Taylor vortices) in the $(r-z)$ plane. Figure 2 shows the computed steady-state streamlines and vorticity field for the case $\sigma = 0$. It is noted that five pairs of counter-rotating cells are present, corresponding to a non-dimensional wave number $a = \pi r_o/\lambda = 6{\cdot}283$. This compares quite well to the value found for an infinitely long annulus of $a = 6{\cdot}4$.[7]

Steady-state results showing the onset and subsequent development of the secondary flow as σ is gradually varied are shown next. First, the steady-state solution for the case $\sigma = 10$ was found, with the heating and rotation of the inner cylinder started impulsively. Then, σ was gradually reduced, using the results of the previous run as initial conditions. All of the results for $\sigma > 1{\cdot}0$ closely resemble the pure natural convection flow patterns (with $Re = 0$). These results are discussed in a previous study.[2,3] The first appearance of a Taylor vortex occurred at $\sigma = 1{\cdot}0$, and can be seen at the top of the annulus in Figure 3. The secondary flow for this state consists of a large vortex rotating in the positive sense, with a small counter-rotating (negative) vortex at the top of the annulus. For the sake of clarity in this discussion, a vortex will be considered to have a positive sense when its rotation is in the same sense as the natural convection flow, i.e. when the flow immediately adjacent to the heated inner cylinder is in the upward (positive z) direction. At $\sigma = 1{\cdot}0$, the buoyancy still dominates the flow, and thus the positive vortex is much larger than the upper negative vortex. The negative vortex is the first manifestation of the presence of the Taylor instability.

The next bifurcation in the flow, from a one-pair to a three-pair Taylor cell state, occurs at $\sigma = 0{\cdot}1$. The three-pair state is shown in Figure 4. In each of the three pairs of counter-rotating

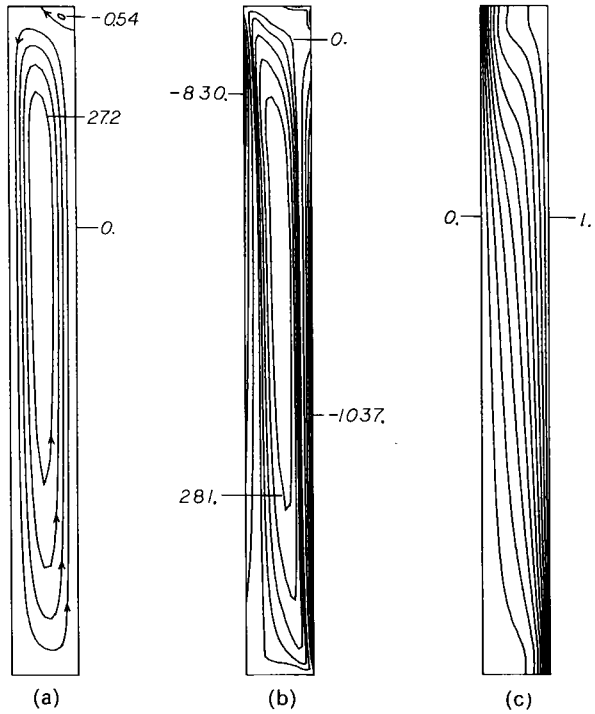

Figure 3. (a) Streamlines, $\pm \Delta\psi = 6{\cdot}8$, $-\Delta\psi = 0{\cdot}11$, (b) vorticity field, $+\Delta\omega = 70{\cdot}2$, $-\Delta\omega = 207{\cdot}5$, and (c) temperature field, $\Delta T = 0{\cdot}1$ for $Re = 100$, $\sigma = 1{\cdot}0$

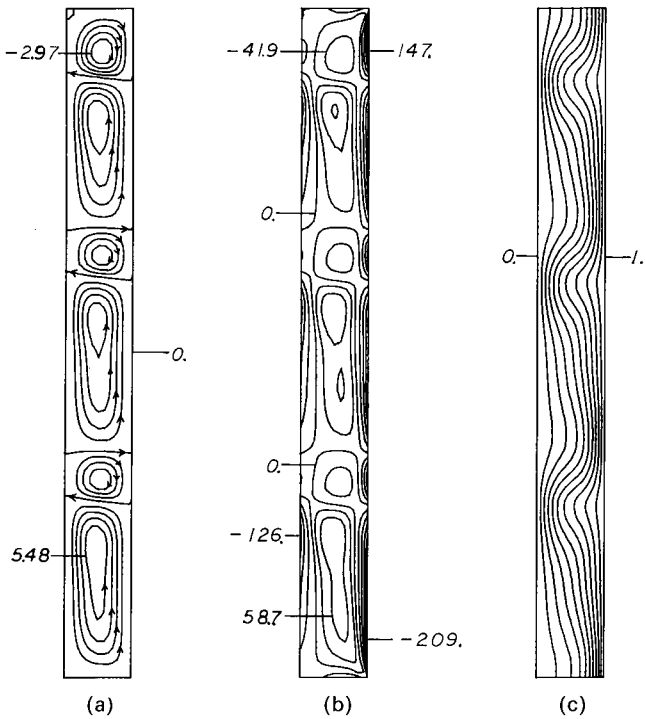

Figure 4. (a) Streamlines, $+\Delta\psi = 1{\cdot}4$, $-\Delta\psi = 0{\cdot}74$, (b) vorticity field, $+\Delta\omega = 32{\cdot}5$, $-\Delta\omega = 36{\cdot}7$, and (c) temperature field, $\Delta T = 0{\cdot}1$ for $Re = 100$, $\sigma = 0{\cdot}1$

cells, the positive cell is much larger. This is due to the influence of the buoyancy force. Even at $\sigma = 0{\cdot}1$, the tendency of the warmer fluid particles adjacent to the heated inner cylinder to rise is sufficiently strong to overcome the regular spacing characteristic of the Taylor instability. Furthermore, it is significant that the positive cell is the larger cell. Referring back to Figure 2, it is observed that the cell at the top of the annulus has a negative sense, whereas the bottom cell has a positive sense. When buoyancy is introduced into the flow, the extra vorticity induced by the natural convection circulation assists the positive Taylor cells, causing them to grow, while at the same time reducing the magnitude of the vorticity of the negative Taylor cells, which diminish in size. Hence, the bottom cell is expected to grow, while the top cell remains small, as the influence of buoyancy (characterized by σ) increases.

In Figure 4, it is also observed that each pair of counter-rotating cells occupies the same volume; namely, one-third of the annulus. In the bottom two pairs, the positive cell is approximately 4·75 times as large as the negative cell. However, the uppermost pair of cells has a size ratio of 2·46. This is due to the fact that the magnitude of the buoyancy-induced vorticity is relatively small at the top of the annulus (compared to the middle where it reaches a maximum). Thus, the negative vorticity induced by the Taylor instability at the top of the annulus is diminished the least by the buoyancy there (which induces vorticity with a positive sense). This also explains why the first appearance of a Taylor cell occurs at the top of the annulus, as shown in Figure 3, in contrast to the isothermal case. In the isothermal flow, the Taylor cells develop from Ekman rolls, which grow from both ends of the annulus and eventually meet in the centre to form a flow pattern which is symmetric about the mid-plane.[8,12,13]

It is interesting to note that a stable, two-pair Taylor cell state was never observed. This can also be explained by observing the interaction of the vorticity induced by the buoyancy forces with the vorticity resulting from the Taylor instability. Since the positive vorticity induced by the buoyancy forces alone reaches a maximum near the mid-plane of the annulus, a negative Taylor cell would be unlikely to develop there. The three-pair state which does develop thus represents a lower energy state than the two-pair mode.

The next bifurcation in the flow, from a three-pair to a four-pair Taylor cell state, occurs just below $\sigma = 0{\cdot}1$. The four-pair state persists down to $\sigma = 0{\cdot}05$, where it is replaced by the five-pair state characteristic of the isothermal flow. Below $\sigma = 0{\cdot}05$, the flow is dominated by the rotational forces, and the buoyancy has very little effect on the flow. The four-pair and five-pair Taylor cell states are shown in Figures 5 and 6, respectively.

In Figures 3(c)–6(c), the effect of the secondary flow on the temperature distribution is plainly seen. The counter-rotating Taylor vortices greatly assist the transport of fluid across the annular gap. The mean equivalent conductivity $\bar{k}_{eq}$ is a measure of the effectiveness of the heat-transport mechanism. The variation of $\bar{k}_{eq}$ with σ is shown in Figure 7. The higher wave-number states clearly have a more effective transport mechanism. Hence, the expected decrease in $\bar{k}_{eq}$ with σ is dramatically changed at each bifurcation to a different state. Figure 7 thus reveals the bifurcation behaviour of the flow with respect to variations in the rotational parameter σ.

The development of the Taylor vortices in the mixed-convection mode with time, with impulsively started heating and rotation, closely parallels the evolution of the secondary flow with decreasing values of σ. Figure 8 shows the development of the flow for $\sigma = 0{\cdot}1$ at different times, identified by the Fourier number Fo. It is observed that the Taylor cell structure also develops at the top of the annulus. Since the Prandtl number for air, $Pr = 0{\cdot}7$, is less than unity, the buoyancy forces dominate the flow for small values of Fo. As the flow develops with increasing time, the relatively slower diffusion of momentum eventually dominates the flow, and the three-cell structure is observed after a sufficient period of time.

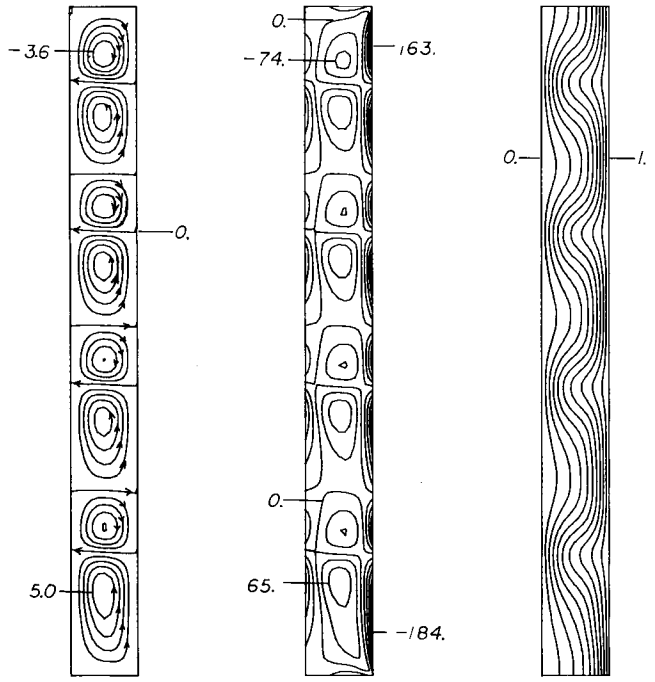

Figure 5. (a) Streamlines, $+\Delta\psi = 1{\cdot}3$, $-\Delta\psi = 0{\cdot}89$, (b) vorticity field, $+\Delta\omega = 32{\cdot}5$, $-\Delta\omega = 36{\cdot}7$, and (c) temperature field, $\Delta T = 0{\cdot}1$ for $Re = 100$, $\sigma = 0{\cdot}05$

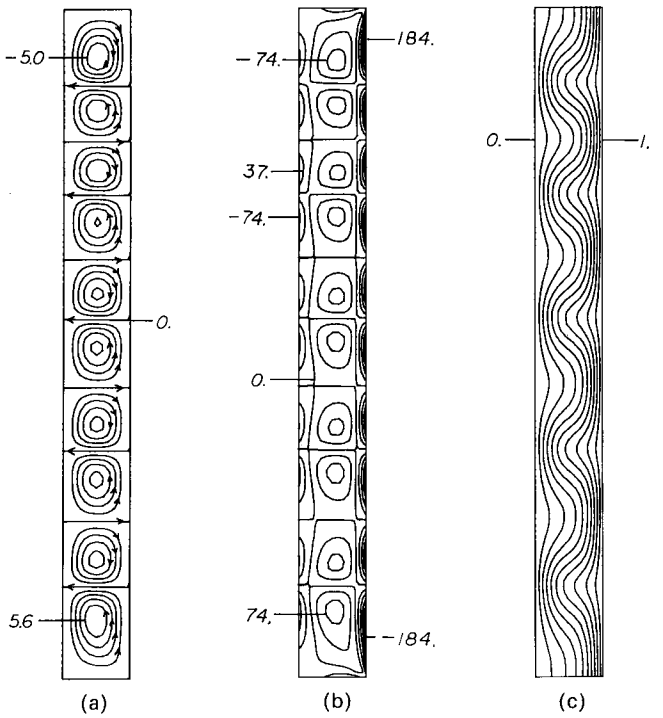

Figure 6. (a) Streamlines, $+\Delta\psi = 1{\cdot}1$, $-\Delta\psi = 1{\cdot}0$, (b) vorticity field, $\pm\Delta\omega = 36{\cdot}8$ and (c) temperature field, $\Delta T = 0{\cdot}1$ for $Re = 100$, $\sigma = 0{\cdot}01$

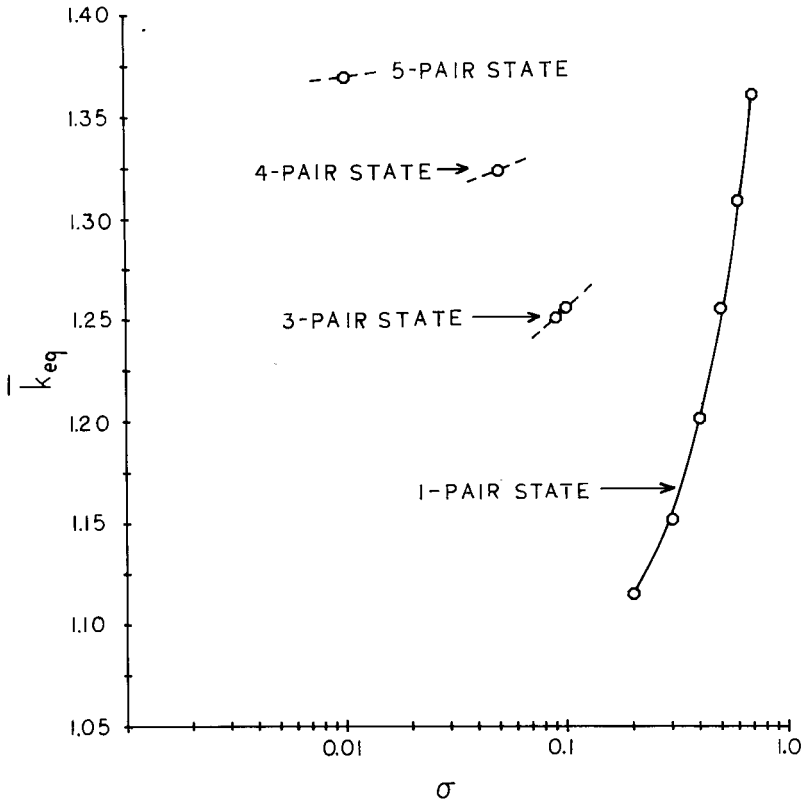

Figure 7. Mean equivalent conductivity variation with σ for $Re = 100$

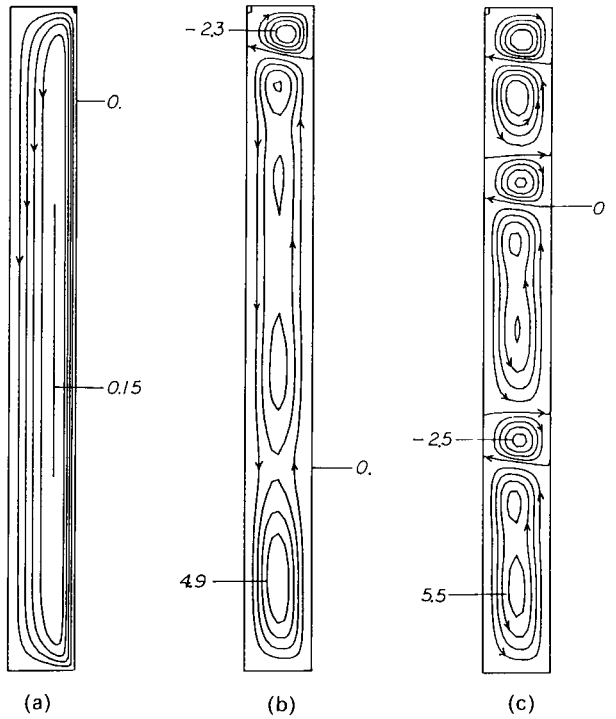

Figure 8. Streamlines showing the transient development of the flow for $Re = 100$, $\sigma = 0{\cdot}1$: (a) $Fo = 0{\cdot}00618$, (b) $Fo = 0{\cdot}5562$, (c) $Fo = 1{\cdot}9208$

CONCLUSION

In this paper, the effects that the introduction of buoyancy has on the development of the Taylor-vortex flow have been studied. Several important conclusions have been reached. First, the formation of the Taylor vortices is suppressed by the buoyancy for values of the rotational parameter $\sigma = Gr/Re^2$ greater than unity. Below $\sigma = 1{\cdot}0$, Taylor vortices first appear, with the cells developing at the top of the annulus. As the parameter σ is slowly decreased, a succession of different states, characterized by distinct (and increasing) wave numbers, is found to exist. In the mixed-convection region ($0{\cdot}01 < \sigma < 1{\cdot}0$), a 'distorted' form of the Taylor cells is observed, with the cell rotating in the same sense as the natural convection circulation (the positive cell) being larger than the other cell in the counter-rotating pair. As σ was decreased below $\sigma = 0{\cdot}01$, the isothermal flow patterns were eventually recovered.

NOMENCLATURE

a non-dimensional wave number ($= \pi r_o/\lambda$)
A acceleration ratio ($= \Omega^2 r_i/g$)
c_p specific heat
d gap width ($= r_o - r_i$)
Fo Fourier number ($= tv/d^2$)
Gr Grashof number ($= d^3\beta g(T_i - T_o)/v^2$)
h heat transfer coefficient
H height of annulus
k thermal conductivity
k_{eq} local equivalent conductivity ($= (hr/k)\ln(r_o/r_i)$)
k_{eq} mean equivalent conductivity
Pr Prandtl number ($= v/\alpha$)
r cylinder radius
Re rotational Reynolds number ($= r_i\Omega d/v$)
t time
T temperature
Ta Taylor number ($= 4\Omega^2 r_i^4/(v(1-\eta^2))^2$)
α thermal diffusivity ($= k/\rho c_p$)
β thermal coefficient of volumetric expansion
Γ aspect ratio ($= H/d$)
η radius ratio ($= r_i/r_o$)
λ wavelength of Taylor cells (axial length of a single cell)
μ viscosity
v kinematic viscosity ($= \mu/\rho$)
ρ density
σ densiometric Froude number ($= Gr/Re^2$)
ψ stream function
ω vorticity
Ω angular speed of rotation of inner cylinder (rad/sec)

Subscripts

crit critical values.
i conditions applying at inner cylinder
o conditions applying at outer cylinder

REFERENCES

1. F. Kreith, 'Convection heat transfer in rotating systems', in *Advances in Heat Transfer 5*, Academic Press, New York, 1968, pp. 129–251.
2. H. P. Greenspan, *The Theory of Rotating Fluids*, Cambridge University Press, New York, 1968.
3. P. H. Singer, 'Techniques of low pressure chemical vapor deposition', *Semiconductor International*, May 1984, pp. 72–77.
4. J. T. Stuart, 'On the non-linear mechanics of hydrodynamic stability', *J. Fluid Mech.*, **4,** 1–21 (1958).
5. G. I. Taylor, 'Stability of a viscous liquid contained between two rotary cylinders', *Phil. Trans. Roy. Soc. A.* **223,** 289–343 (1923).
6. D. Coles, 'Transition in circular couette flow', *J. Fluid Mech.*, **21,** (part 3), 385–425 (1965).
7. S. Chandrasekhar, *Hydrodynamic and Hydromagnetic Stability*, Dover Publications, New York, 1981.
8. T. B. Benjamin and T. Mullin, 'Notes on the multiplicity of flows in the Taylor experiment', *J. Fluid Mech.*, **121,** 219–230 (1982).
9. T. Mullin, 'Mutations of steady cellular flows in the Taylor experiment', *J. Fluid Mech.*, **121,** 207–218 (1982).
10. K. A. Cliffe, 'Numerical calculations of two-cell and single-cell Taylor flows', *J. Fluid Mech.*, **135,** 219–233 (1983).
11. C. T. Hughes, E. Leonardi, G. de Vahl Davis and J. A. Reizes, 'A numerical study of the multiplicity of flows in the Taylor experiment', *Physico Chemical Hydrodynamics*, **6,** 637–645 (1985).
12. G. Ahlers and D. S. Cannell, 'Vortex-front propagation in rotating couette-Taylor flow', *Phys. Rev. Lett.*, **50,** 1583–1586 (1983).
13. G. P. Neitzel, 'Numerical computation of time-dependent Taylor-vortex flows in finite-length geometries', *J. Fluid Mech.*, **141,** 51–66 (1984).
14. J. E. Burkhalter and E. L. Koschmieder, 'Steady supercritical Taylor vortex flow', *J. Fluid Mech.*, **58,** 547–560 (1973).
15. T. Alziary de Roquefort and G. Grillaud, 'Computation of Taylor vortex flow by a transient implicit method', *Comp. Fluids*, **6,** 259–269 (1978).
16. H. A. Snyder, 'Wave-number selection at finite amplitude in rotating couette flow', *J. Fluid Mech.*, **35,** 273–298 (1969).
17. H. A. Snyder and S. K. F. Karlsson, 'Experiments on the stability of couette motion with a radical thermal gradient', *Phys. Fluids*, **7,** 1696–1706 (1964).
18. H. A. Snyder, 'Experiments on the stability of two types of spiral flow', *Ann. Phys.*, **31,** 292–313 (1965).
19. S. K. F. Karlsson and H. A. Snyder, 'Observations on a thermally induced instability between rotating cylinders', *Ann. Phys.*, **31,** 314–324 (1965).
20. G. de Vahl Davis, E. Leonardi and J. A. Reizes, 'Convection in a rotating annular cavity', in Metzger and Afgan (eds), *Heat and Mass Transfer in Rotating Machinery*, Hemisphere Publishing, 1984, pp. 131–142.
21. E. Leonardi, J. A. Reizes and G. de Vahl Davis, 'Heat transfer in a vertical rotating annulus—a numerical study', *Proc. 7th Int. Heat Trans. Conf.*, Vancouver, 1982, Paper FC12.
22. B. Gebhart, Y. Jaluria, R. Mahajan and B. Sammakia, *Buoyancy Induced Flows and Transport* (in press).
23. K. S. Ball and B. Farouk, 'Numerical studies of mixed convection flows in the annulus between vertical concentric cylinders with rotating inner cylinder', *Proc. 8th Int. Heat Trans. Conf.*, San Francisco, 1986, pp. 435–440.